JOURNAL OF MOLECULAR SPECTROSCOPY 85, 120–130 (1981)

A Study of the Rotational–Torsional Spectrum of Hydrogen Peroxide between 80 and 700 GHz[1]

PAUL HELMINGER

Department of Physics, University of South Alabama, Mobile, Alabama 36688

AND

WAYNE C. BOWMAN AND FRANK C. DE LUCIA

Department of Physics, Duke University, Durham, North Carolina 27706

One hundred and thirty-three new rotational transitions that occur between pairs of torsional sublevels in the ground vibrational state of hydrogen peroxide have been measured in the 80 to 700 GHz region of the spectrum. These data, in combination with the 50 previously measured lines, have been theoretically analyzed to within the expected experimental uncertainty ($\lesssim$0.1 MHz). The rotational constants for the τ = 1, 2 state are (in MHz): A = 301 878.857 ± 0.015, B = 26 211.9019 ± 0.0059, C = 25 099.1400 ± 0.0059, and for the τ = 3, 4 state: A = 301 583.825 ± 0.075, B = 26 156.337 ± 0.13, C = 25 185.771 ± 0.13. The splitting between the torsional levels is 342 885.03 ± 0.05. These measurements and analysis accurately characterize the nine branches that make substantial contributions in the spectral region below 700 GHz.

INTRODUCTION

Hydrogen peroxide occurs commonly in a variety of important physical and chemical systems including those associated with upper atmospheric and combustion processes. It is the simplest molecule that can execute torsional motion, and as a light asymmetric rotor has substantial centrifugal distortion contributions to its rotational–torsional spectrum. The millimeter and submillimeter studies reported here provide both fundamental spectroscopic information and data important for remote sensing and atmospheric transmission calculations.

A number of infrared and far-infrared studies of HOOH have been reported (*1–4*) and provide a framework for the analysis and interpretation of the work reported here. Massey and his co-workers (*5, 6*) have reported the measurement and assignment of two lines in the microwave region, and Oelfke and Gordy (*7*) have published a study based upon 50 millimeter-wave transitions. The complexity of this spectrum has precluded an accurate, self-consistent analysis of these data.

This work reports the measurement of 133 new rotation–torsion lines between 80 and 700 GHz, the assignment of four previously unassigned lines of Oelfke

[1] This work supported by NASA Grant NSG-7540.

0022-2852/81/010120-11$02.00/0

(*8*), corrections to four previously measured microwave and millimeter-wave lines, measurement of three new branches and the substantial extension of six others, and the first analysis of this data to within experimental uncertainty (~0.1 MHz) in the context of an accurate, compact asymmetric rotor formalism.

EXPERIMENTAL DETAILS

We have discussed our general experimental techniques previously (*9*). For this work, the sample cell was a 1-m-long, 2.5-cm-diameter copper pipe with teflon windows. The interior of the pipe was coated with clear Krylon to inhibit chemical decomposition. Typical sample pressure was 0.020 Torr. Except for eight weakly absorbing lines, all data were measured in real time on an oscilloscope.

SPECTRUM AND ENERGY LEVELS

Structurally, HOOH is similar to HSSH, whose microwave spectrum has been extensively studied by Winnewisser and co-workers (*10–13*). An extensive set of high-accuracy data was obtained and carefully analyzed. However, two spectroscopic differences are significant and complicate the HOOH problem: (1) The barriers to internal rotation in HSSH are substantially higher, thereby effectively removing internal rotation effects from consideration, and (2) HSSH is almost exactly an accidental symmetric top ($\kappa = -0.99996$).

HOOH should be considered as a member of a more general class of molecules in which low-lying vibrational modes (e.g., inversions, internal rotations, low-lying bends, etc.) interact with rotational energy level structures and spectra. In many ways the species that most closely resemble HOOH spectroscopically are NH_2D and ND_2H (*14*). All are light asymmetric rotors and as such require a careful centrifugal distortion treatment. In addition, the inversion barrier of the ammonia species produces a splitting similar to, but smaller than, the torsional splittings in HOOH.

Figure 1 shows that HOOH has a high *cis* barrier to internal rotation and a much lower *trans* barrier (*4*). As a result, the fourfold degeneracy of the lowest torsional state ($n = 0$) is broken and a doublet of doublets occurs, the smaller splitting determined by the high *cis* barrier and the larger splitting by the lower *trans* barrier. These four sublevels are designated $\tau = 1, 2, 3, 4$ in order of increasing energy. Because of symmetry conditions associated with the torsional motion, rotational states are distributed among the four torsional states according to the evenness or oddness of the K_{-1} rotational quantum number (*4*). These assignments are also shown in Fig. 1.

The selection rules can be obtained from a consideration of the matrix elements of the electric dipole moment, which for HOOH lies along the c axis. Its component along a space fixed Z axis is

$$\mu_Z = \Phi_{Zc}\mu_c, \tag{1}$$

where Φ_{Zc} is the direction cosine. The matrix elements are

$$(J,K_{-1},K_1,\tau|\mu_Z|J'_1,K'_{-1},K'_1,\tau') = (J,K_{-1},K_1|\Phi_{Zc}|J',K'_{-1},K'_1)(\tau|\mu_c|\tau'), \tag{2}$$

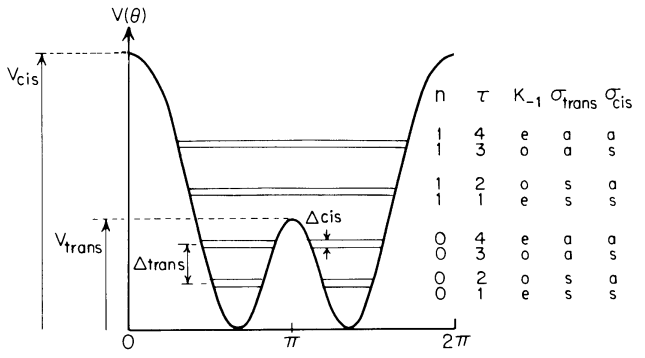

FIG. 1. Torsional potential and symmetry labeling of HOOH.

where J, K_{-1}, and K_1 specify the rotational state, and τ specifies the torsional state. The matrix elements of the direction cosine give rise to the usual c-type asymmetric rotor selection rules, while the matrix elements of the body fixed dipole moment represent restrictions on transitions between torsional levels. These restrictions can be determined from a consideration of the symmetry properties, shown in Fig. 1, of the torsional wave functions. Because σ_{cis} does not change the sign of μ_c, while σ_{trans} does, $(\tau|\mu_c|\tau')$ can be nonzero only for transitions for which both

$$\sigma_{trans}: \quad s \leftrightarrow a'; \quad a \leftrightarrow s',$$

$$\sigma_{cis}: \quad s \leftrightarrow s'; \quad a \leftrightarrow a'.$$

From Fig. 1, the selection rules become

$$\tau: \quad 1 \leftrightarrow 3; \quad 2 \leftrightarrow 4.$$

As a consequence, under the zeroth-order assumption that the rotational constants in all four states are identical and that $\tau_{1,2}$ and $\tau_{3,4}$ are degenerate, two complete sets of c-type asymmetric rotor transitions exist; one offset by the torsional splitting (~340 GHz) to higher frequency and the other offset by a similar amount to lower frequency. Figure 2 shows a FORTRAT diagram of the observed data points. Table I records these data in tabular form.

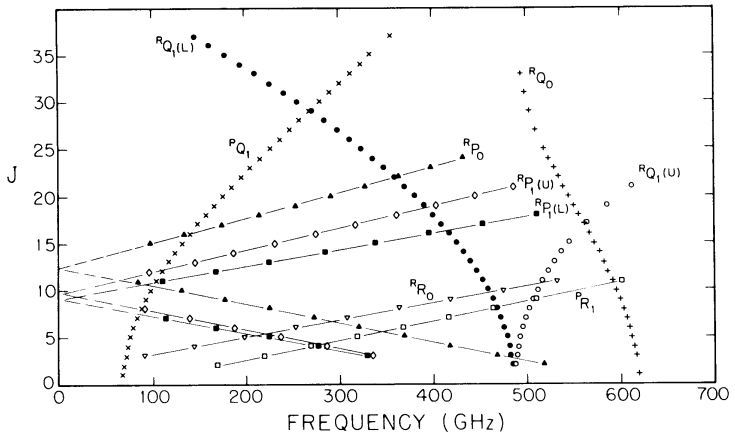

FIG. 2. FORTRAT diagram of the observed branches of HOOH.

TABLE I

Observed Transitions of HOOH (MHz)

P_{Q_1} Branch Transitions

Transition			Frequency
$\tau = 2$		$\tau = 4$	Observed
1_{11}	-	1_{01}	67 245.73
2_{12}	-	2_{02}	68 385.02
3_{13}	-	3_{03}	70 090.22
4_{14}	-	4_{04}	72 356.40
5_{15}	-	5_{05}	75 177.43
6_{16}	-	6_{06}	78 545.43
7_{17}	-	7_{07}	82 450.84
8_{18}	-	8_{08}	86 882.75
9_{19}	-	9_{09}	91 828.60
10_{110}	-	10_{010}	97 274.01
11_{111}	-	11_{011}	103 203.59
12_{112}	-	12_{012}	109 599.96
13_{113}	-	13_{013}	116 444.45
14_{114}	-	14_{014}	123 716.95
15_{115}	-	15_{015}	131 396.11
16_{116}	-	16_{016}	139 459.44
17_{117}	-	17_{017}	147 882.98
18_{118}	-	18_{018}	156 642.42
19_{119}	-	19_{019}	165 712.17
20_{120}	-	20_{020}	175 066.56
21_{121}	-	21_{021}	184 679.22
22_{122}	-	22_{022}	194 523.88
23_{123}	-	23_{023}	204 574.70
24_{124}	-	24_{024}	214 805.95
25_{125}	-	25_{025}	225 193.00
26_{126}	-	26_{026}	235 712.16
27_{127}	-	27_{027}	246 341.39
28_{128}	-	28_{028}	257 059.57
29_{129}	-	29_{029}	267 848.56
30_{130}	-	30_{030}	278 691.28
31_{131}	-	31_{031}	289 573.70
32_{132}	-	32_{032}	300 483.98
33_{133}	-	33_{033}	311 412.37
34_{134}	-	34_{034}	322 352.51
35_{135}	-	35_{035}	333 300.02
36_{136}	-	36_{036}	(344 253.47)[a]
37_{137}	-	37_{037}	355 213.25

R_{R_0} Branch Transitions

Transition			Frequency
$\tau = 2$		$\tau = 4$	
1_{10}	-	0_{00}	14 829.5[b]
2_{11}	-	1_{01}	37 517.6[b]
3_{12}	-	2_{02}	90 365.32
4_{13}	-	3_{03}	143 712.66
5_{14}	-	4_{04}	197 561.30
6_{15}	-	5_{05}	251 914.71
7_{16}	-	6_{06}	306 777.58
8_{17}	-	7_{07}	362 156.21
9_{18}	-	8_{08}	418 058.49
10_{19}	-	9_{09}	474 493.46
11_{110}	-	10_{010}	531 471.83
12_{111}	-	11_{011}	589 005.83

P_{R_1} Branch Transitions

Transition			Frequency
$\tau = 4$		$\tau = 2$	
2_{02}	-	1_{10}	168 849.54
3_{03}	-	2_{11}	219 166.86
4_{04}	-	3_{12}	268 961.17
5_{05}	-	4_{13}	318 222.52
6_{06}	-	5_{14}	366 940.43
7_{07}	-	6_{15}	415 102.33
8_{08}	-	7_{16}	462 693.96
9_{09}	-	8_{17}	509 699.93
10_{010}	-	9_{18}	(556 103.43)
11_{011}	-	10_{19}	601 885.28

a. Numbers in parentnesis are calculated from the constants of Table II.

b. From ref. 5.

ANALYSIS OF THE SPECTRUM

Prior work has emphasized the roll of torsional motion, with lesser consideration of the effects of molecular asymmetry and centrifugal distortion. This has been because infrared and far-infrared spectroscopy directly observes the most important manifestation of this motion, the torsional splittings. Because of the lower resolution of these techniques, the experimental data could be analyzed without recourse to detailed asymmetric rotor theory. However, in the millimeter

TABLE I—*Continued*

R_{P_0} Branch Transitions

Transition			Frequency
$\tau = 1$		$\tau = 3$	
$^{2}_{02}$	-	$^{1}_{10}$	516 669.31
$^{3}_{03}$	-	$^{2}_{11}$	466 379.11
$^{4}_{04}$	-	$^{3}_{12}$	416 613.58
$^{5}_{05}$	-	$^{4}_{13}$	367 386.06
$^{6}_{06}$	-	$^{5}_{14}$	318 712.10
$^{7}_{07}$	-	$^{6}_{15}$	270 610.10
$^{8}_{08}$	-	$^{7}_{16}$	223 100.95
$^{9}_{09}$	-	$^{8}_{17}$	176 207.86
$^{10}_{010}$	-	$^{9}_{18}$	129 956.57
$^{11}_{011}$	-	$^{10}_{19}$	84 375.19
$^{12}_{012}$	-	$^{11}_{110}$	(39 494.60)
$^{13}_{013}$	-	$^{12}_{111}$	(4 653.47)
$^{14}_{014}$	-	$^{13}_{112}$	(48 034.07)
$^{15}_{015}$	-	$^{14}_{113}$	90 611.01
$^{16}_{016}$	-	$^{15}_{114}$	132 345.62
$^{17}_{017}$	-	$^{16}_{115}$	173 198.83
$^{18}_{018}$	-	$^{17}_{116}$	213 130.25
$^{19}_{019}$	-	$^{18}_{117}$	252 098.75
$^{20}_{020}$	-	$^{19}_{118}$	290 062.95
$^{21}_{021}$	-	$^{20}_{119}$	326 981.47
$^{22}_{022}$	-	$^{21}_{120}$	362 813.63
$^{23}_{023}$	-	$^{22}_{121}$	397 519.63
$^{24}_{024}$	-	$^{23}_{122}$	431 061.36

R_{P_1} (Lower) Branch Transitions

Transition			Frequency
$\tau = 3$		$\tau = 1$	
$^{3}_{12}$	-	$^{2}_{20}$	328 949.38
$^{4}_{13}$	-	$^{3}_{21}$	275 639.63
$^{5}_{14}$	-	$^{4}_{22}$	221 849.93
$^{6}_{15}$	-	$^{5}_{23}$	167 596.04
$^{7}_{16}$	-	$^{6}_{24}$	112 896.01
$^{8}_{17}$	-	$^{7}_{25}$	(57 770.76)
$^{9}_{18}$	-	$^{8}_{26}$	(2 245.33)
$^{10}_{19}$	-	$^{9}_{27}$	(53 653.17)
$^{11}_{110}$	-	$^{10}_{28}$	109 893.97
$^{12}_{111}$	-	$^{11}_{29}$	166 443.99
$^{13}_{112}$	-	$^{12}_{210}$	223 267.04
$^{14}_{113}$	-	$^{13}_{211}$	280 323.36
$^{15}_{114}$	-	$^{14}_{212}$	337 571.21
$^{16}_{115}$	-	$^{15}_{213}$	394 966.03
$^{17}_{116}$	-	$^{16}_{214}$	452 460.90
$^{18}_{117}$	-	$^{17}_{215}$	510 006.35

R_{P_1} (Upper) Branch Transitions

Transition			Frequency
$\tau = 3$		$\tau = 1$	
$^{3}_{13}$	-	$^{2}_{21}$	334 606.69
$^{4}_{14}$	-	$^{3}_{22}$	285 058.26
$^{5}_{15}$	-	$^{4}_{23}$	235 956.09
$^{6}_{16}$	-	$^{5}_{24}$	187 302.82
$^{7}_{17}$	-	$^{6}_{25}$	139 102.38
$^{8}_{18}$	-	$^{7}_{26}$	91 357.98
$^{9}_{19}$	-	$^{8}_{27}$	(44 073.01)
$^{10}_{110}$	-	$^{9}_{28}$	(2 748.80)
$^{11}_{111}$	-	$^{10}_{29}$	(49 103.94)
$^{12}_{112}$	-	$^{11}_{210}$	94 988.63
$^{13}_{113}$	-	$^{12}_{211}$	140 399.47
$^{14}_{114}$	-	$^{13}_{212}$	185 333.30
$^{15}_{115}$	-	$^{14}_{213}$	229 785.93
$^{16}_{116}$	-	$^{15}_{214}$	273 754.05
$^{17}_{117}$	-	$^{16}_{215}$	317 234.35
$^{18}_{118}$	-	$^{17}_{216}$	360 223.46
$^{19}_{119}$	-	$^{18}_{217}$	402 718.27
$^{20}_{120}$	-	$^{19}_{218}$	444 715.93
$^{21}_{121}$	-	$^{20}_{219}$	486 212.93

R_{Q_1} (Upper) Branch Transitions

Transition			Frequency
$\tau = 1$		$\tau = 3$	
$^{2}_{20}$	-	$^{2}_{12}$	487 202.04
$^{3}_{21}$	-	$^{3}_{13}$	488 516.11
$^{4}_{22}$	-	$^{4}_{14}$	490 282.51
$^{5}_{23}$	-	$^{5}_{15}$	492 513.18
$^{6}_{24}$	-	$^{6}_{16}$	495 223.22
$^{7}_{25}$	-	$^{7}_{17}$	498 430.80
$^{8}_{26}$	-	$^{8}_{18}$	502 157.04
$^{9}_{27}$	-	$^{9}_{19}$	506 426.02
$^{10}_{28}$	-	$^{10}_{110}$	511 264.49
$^{11}_{29}$	-	$^{11}_{111}$	516 702.35
$^{12}_{210}$	-	$^{12}_{112}$	522 772.00
$^{13}_{211}$	-	$^{13}_{113}$	529 508.25
$^{14}_{212}$	-	$^{14}_{114}$	536 948.96
$^{15}_{213}$	-	$^{15}_{115}$	545 133.67
$^{16}_{214}$	-	$^{16}_{116}$	(554 103.93)
$^{17}_{215}$	-	$^{17}_{117}$	563 903.81
$^{18}_{216}$	-	$^{18}_{118}$	(574 578.23)
$^{19}_{217}$	-	$^{19}_{119}$	586 173.39
$^{20}_{218}$	-	$^{20}_{120}$	(598 735.42)
$^{21}_{219}$	-	$^{21}_{121}$	612 312.12

and submillimeter spectral region, the rolls played by rotation and centrifugal distortion become dominant.

As discussed above, the spectrum of HOOH is that of a slightly asymmetric rotor that simultaneously undergoes both a torsional and a rotational transition.

TABLE I—*Continued*

R_{Q_1} (Lower) Branch Transitions			R_{Q_0} Branch Transitions		
Transition		Frequency	Transition		Frequency
$\tau = 1$	$\tau = 3$		$\tau = 1$	$\tau = 3$	
2_{21} -	2_{11}	484 369.02	1_{01} -	1_{11}	618 341.76
3_{22} -	3_{12}	482 841.43	2_{02} -	2_{12}	(617 458.93)
4_{23} -	4_{13}	480 805.26	3_{03} -	3_{13}	616 141.45
5_{24} -	5_{14}	478 281.21	4_{04} -	4_{14}	614 396.80
6_{25} -	6_{15}	475 209.80	5_{05} -	5_{15}	612 235.46
7_{26} -	7_{16}	471 652.00	6_{06} -	6_{16}	609 670.35
8_{27} -	8_{17}	467 568.82	7_{07} -	7_{17}	606 717.52
9_{28} -	9_{18}	463 021.60	8_{08} -	8_{18}	603 394.93
10_{29} -	10_{19}	457 951.65	9_{09} -	9_{19}	599 723.68
11_{210} -	11_{110}	452 380.53	10_{010} -	10_{110}	595 726.87
12_{211} -	12_{111}	446 310.18	11_{011} -	11_{111}	591 430.62
13_{212} -	13_{112}	439 742.65	12_{012} -	12_{112}	586 863.36
14_{213} -	14_{113}	432 680.02	13_{013} -	13_{113}	582 055.95
15_{214} -	15_{114}	425 125.17	14_{014} -	14_{114}	577 041.59
16_{215} -	16_{115}	417 080.79	15_{015} -	15_{115}	571 854.96
17_{216} -	17_{116}	408 550.02	16_{016} -	16_{116}	566 533.53
18_{217} -	18_{117}	399 536.42	17_{017} -	17_{117}	561 116.33
19_{218} -	19_{118}	390 043.90	18_{018} -	18_{118}	555 643.34
20_{219} -	20_{119}	380 076.64	19_{019} -	19_{119}	550 155.92
21_{220} -	21_{120}	369 639.28	20_{020} -	20_{120}	544 696.71
22_{221} -	22_{121}	358 737.00	21_{021} -	21_{121}	539 308.17
23_{222} -	23_{122}	347 375.29	22_{022} -	22_{122}	534 033.18
24_{223} -	24_{123}	335 560.27	23_{023} -	23_{123}	528 914.26
25_{224} -	25_{124}	323 298.60	24_{024} -	24_{124}	523 992.87
26_{225} -	26_{125}	310 597.37	25_{025} -	25_{125}	519 309.79
27_{226} -	27_{126}	297 464.53	26_{026} -	26_{126}	(514 903.72)
28_{227} -	28_{127}	283 908.23	27_{027} -	27_{127}	510 811.59
29_{228} -	29_{128}	269 937.86	28_{028} -	28_{128}	(507 068.20)
30_{229} -	30_{129}	255 563.00	29_{029} -	29_{129}	503 705.44
31_{230} -	31_{130}	240 794.31	30_{030} -	30_{130}	(500 752.77)
32_{231} -	32_{131}	225 642.94	31_{031} -	31_{131}	498 236.38
33_{232} -	33_{132}	210 121.00	32_{032} -	32_{132}	(496 179.70)
34_{233} -	34_{133}	194 241.24			
35_{234} -	35_{134}	178 017.33			
36_{235} -	36_{135}	161 463.74			
37_{236} -	37_{136}	144 595.60			

We find that it is possible to fit all 183 microwave transitions to within their experimental uncertainty (~0.1 MHz) with the Hamiltonian

$$H = H_{\text{rot}} + H_{\text{tor}}, \tag{3}$$

$$\begin{aligned} H_{\text{rot}} = {} & AP_z^2 + BP_x^2 + CP_y^2 - \Delta_J P^4 - \Delta_{JK} P^2 P_z^2 - \Delta_K P_z^4 - 2\delta_J P^2 (P_x^2 - P_y^2) \\ & - \delta_K [P_z^2 (P_x^2 - P_y^2) + (P_x^2 - P_y^2) P_z^2] + H_J P^6 + H_{JK} P^4 P_z^2 \\ & + H_{KJ} P^2 P_z^4 + h_{JK} P^2 [P_z^2 (P_x^2 - P_y^2) + (P_x^2 - P_y^2) P_z^2], \end{aligned} \tag{4}$$

$$H_{\text{tor}} = \alpha(\Theta) P_x^2 + V(\Theta). \tag{5}$$

TABLE II

Rotational Constants (MHz)

	$\tau = 1, 2$		$\tau = 3, 4$	
	value	σ	value	σ
A	301 878.857	0.015	301 583.825	0.076
B	26 211.9019	0.0059	26 156.337	0.13
C	25 099.1400	0.0059	25 185.771	0.13
$\Delta_J(\cdot 10^0)$	0.105277	0.000013	0.099620	0.000053
$\Delta_{JK}(\cdot 10^1)$	0.112497	0.000027	0.127304	0.0018
$\Delta_K(\cdot 10^2)$	0.132000	a	0.132000	a
$\delta_J(\cdot 10^{-3})$	-0.2618	0.0139	1.042	0.051
$\delta_K(\cdot 10^1)$	0.947345	0.00023	0.679089	0.0066
$H_J(\cdot 10^{-7})$	-0.32	0.19	2.053	0.24
$H_{JK}(\cdot 10^{-3})$	0.37095	0.00092	0.2072	0.0071
$H_{KJ}(\cdot 10^0)$	------		0.1224	0.016
$h_{JK}(\cdot 10^{-3})$	0.168	0.009	0.46647	0.047
rms	0.119		0.106	
number of independent data points	71		96	
W	342 885.03			

a. Value fixed from infrared data.

The rotational part of this Hamiltonian is the usual Watson (*15*) formulation of the asymmetric rotor centrifugal distortion problem. Although fundamental formulations of the problem indicate the existence (if not the magnitude) of rotational–torsional cross terms, we conclude that contributions from these are either negligibly small or highly correlated with contributions from terms of our Hamiltonian. As a result, the torsional Hamiltonian is diagonal and simply contributes a torsional energy, W.

For the purposes of analysis, we assume (the implications of and reasons for this assumption are discussed below) that the rotational constants in the states $\tau = 1, 2$ are identical, and we make the same assumption for the states $\tau = 3, 4$. However, because the constants in $\tau = 1, 2$ differ from those in $\tau = 3, 4$, we have adopted an analysis technique similar to that commonly used for the analysis of infrared vibration–rotation spectra. Ground state ($\tau = 1, 2$) combination differences are produced by subtraction between the ${}^PQ_1/{}^PR_1$, ${}^RR_0/{}^PQ_1$, ${}^RP_1(L)/{}^RP_0$, ${}^RQ_1(L)/{}^RP_1(L)$, ${}^RQ_1(U)/{}^RP_1(U)$, and ${}^RQ_1(U)/{}^RQ_0$ branches, which have common upper-state energy levels. An asymmetric rotor distortion analysis is then performed on these data and the rotational constants that result from this analysis are shown in Table II. The energy levels which result from this analysis and all of the experimental data are combined to produce energy levels in the $\tau = 3, 4$ state. The result of a centrifugal distortion analysis of these states is also shown in Table II. We find the vibrational splitting between $\tau = 1, 2$ and $\tau = 3, 4$ to be $W = 342\ 885.03$ MHz (11.437412 cm^{-1}).

TABLE III

Comparisons with Earlier Results (MHz)

	this work		reference 7		reference 3		reference 4
	value	σ	value	σ	value	σ	value
$\tau = 1,2$							
A	301 878.86	0.02	301 870.1	2.8	301 831	150	301 633
B	26 211.902	0.006	26 205.1	2.1	26 202	40	26 208
C	25 099.140	0.006	25 119.1	2.1	25 135	40	25 200
Δ_J	0.10528	0.00001	0.116	0.02	0.1349		---
Δ_{JK}	1.1250	0.0003	3.14	0.3	-0.60		---
Δ_K	----		----		22		13
$\tau = 3,4$							
A	301 583.83	0.08	301 586.4	2.8	301 831	150	301 453
B	26 156.34	0.13	26 150.3	2.1	26 202	40	26 148
C	25 185.77	0.13	25 197.1	2.1	25 135	40	25 261
Δ_J	0.09962	0.00005	0.115	0.02	0.1349		---
Δ_{JK}	1.27	0.02	-2.42	0.3	-0.60		---
Δ_K	----		----		22		13
	this work		reference 7		reference 3		reference 4
	value	σ	value	σ	value	σ	value
$W_{3,4}-W_{1,2}$	342 885.03	0.05	342 885.0	2.0	342 963		342 663

It is difficult to make meaningful comparisons between analyses based upon different theoretical formulations. In such cases, it is best simply to compare coefficients of operators and to bypass issues associated with the physical significance of these constants. Hunt *et al.* (*4*) and Gordy and Oelfke (*7*) report β, ν, and γ rather than A, B, and C. For comparison, we have used

$$\beta = 1/2(B + C),$$

$$\nu = A - 1/2(B + C),$$

$$\gamma = 1/2(B - C).$$

Table III shows this comparison, but only includes the lower-order terms for which values were derived in the earlier work. In general the agreement among the rotational constants and torsional splitting is satisfactory although the more recent results are much more accurate. Substantial differences exist among the distortion terms, especially Δ_{JK}. In the infrared studies, the expected effects are small in comparison to measurement uncertainties and in the earlier microwave studies the data set available, although highly accurate, was limited.

TABLE IV

Comparison of Rotational Constants in $\tau = 1$ and $\tau = 2$

	$\tau = 1,2$ Analysis		$\tau = 2$ Analysis		$\tau = 1$ Analysis	
	value	σ	value	σ	value	σ
A	301 878.857	0.015	302 131.515	217.5	301 878.854	0.007
B	26 211.902	0.007	26 211.902	0.003	26 211.901	0.0006
C	25 099.140	0.007	25 099.141	0.003	25 099.140	0.0006

DISCUSSION

We have assumed that the rotational constants in $\tau = 1$ and $\tau = 2$ are the same. The exceptionally good combination difference fit of our large data set indicates this to be true. However, careful inspection of the structure of the analysis shows that A could vary substantially between $\tau = 1$ and $\tau = 2$ without leading to excessive rms deviation in the fit. As discussed above, only K_{-1} even exists in $\tau = 1$ and only K_{-1} odd exists in $\tau = 2$. Thus for $\tau = 1$, we only have data for which $K_{-1} = 0, 2$. Because H_2O_2 is a near prolate rotor, information about spectral constants that are coefficients of P_z^{2n} operators (i.e., A, Δ_K, H_K . . .) comes primarily from data for which K_{-1} changes. Thus, $\tau = 1$ determines a value for A. In $\tau = 2$, we only have $K_{-1} = 1$ data, and consequently no strong information on A. Although it is true that the $K_{-1} = 1$ splittings provide information about A in the $\tau = 2$ state, the uncertainty in any resulting value would be much greater than any expected differences.

As a test we have analyzed the $\tau = 1$ and $\tau = 2$ combination differences separately, and relevant results are listed in Table IV. For purposes of comparison, the results of the full $\tau = 1, 2$ analysis are repeated from Table II. For each of the other analyses, all distortion constants were fixed at the values of Table II. As expected, in the analysis of $\tau = 2$, A is not well determined, but does overlap our value to within 2σ. However, both B and C are well determined and agree with both the results of the combined $\tau = 1, 2$ analysis and the $\tau = 1$ analysis to parts in 10^8. Similar arguments and results exist for the $\tau = 3$ and $\tau = 4$ states.

The consistency between the P^4 distortion constants of $\tau = 1, 2$ and $\tau = 3, 4$ is also gratifying. This is especially so because the spectral information included in the two analyses is very different. The notable exception to this good agreement is δ_J, but it is highly correlated with several other constants and its value is very sensitive to choice of Hamiltonian terms.

A related issue is that of Δ_K. Although with data in the $K_{-1} = 0, 1, 2$ states of $\tau = 1, 2$ it would appear that both A and Δ_K could be calculated from the data, this is not possible because we have no information about $E_{K_{-1}=0} - E_{K_{-1}=1}$. Thus the value of Δ_K is fixed at the value of Ref. (*4*).

We have also assumed that the torsional splitting between $\tau = 1$ and $\tau = 3$ is equal to the splitting between $\tau = 2$ and $\tau = 4$. As discussed above, $\tau = 3$ contains data for which $K_{-1} = 1$ and $\tau = 4$ contains data for which $K_{-1} = 0$. The difference between the energies of these states determines A. If a splitting ΔW were assumed, it would simply change the value of A by $A' = A + \Delta W$.

TABLE V

Expansion Coefficients for the Q Branch Transitions

	P_{Q_1}	R_{Q_1} (u)	R_{Q_1} (L)	R_{Q_0}
X_0	0.66675539×10^{5}	0.48589707×10^{6}	0.48589703×10^{6}	0.61878441×10^{6}
X_1	0.28534499×10^{3}	0.21674200×10^{3}	$-0.25470273 \times 10^{3}$	$-0.22155037 \times 10^{3}$
X_2	$-0.64955141 \times 10^{-1}$	0.12648275×10^{0}	$0.57333704 \times 10^{-2}$	0.10824466×10^{0}
X_3	$-0.38183723 \times 10^{-5}$	$-0.22323518 \times 10^{-5}$	$0.18942850 \times 10^{-5}$	$0.40466322 \times 10^{-5}$
X_4	$0.10418110 \times 10^{-7}$	$-0.10900343 \times 10^{-7}$	$0.11334722 \times 10^{-9}$	$-0.15445320 \times 10^{-7}$
X_5	$-0.29522169 \times 10^{-11}$	0.0	$-0.35504443 \times 10^{-13}$	$0.37832942 \times 10^{-11}$
X_6	$0.24197045 \times 10^{-15}$	0.0	$-0.46904855 \times 10^{-17}$	$0.86669986 \times 10^{-16}$

APPENDIX

Empirical Characterization of the Microwave Spectrum

In order to aid utilization of the data presented in this work, we have developed a power series representation for the frequencies of each branch. The functional forms of the expansions were obtained by approximating the molecule as a rigid, slightly asymmetric rotor.

All Q branches were fit with a power series of the form

$$f(J) = X_0 + X_1J(J+1) + X_2J^2(J+1)^2 + X_3J^3(J+1)^3 + X_4J^4(J+1)^4 + X_5J^5(J+1)^5 + X_6J^6(J+1)^6$$

and the resulting coefficients are shown in Table V.

For the P and R branch transitions a power series of the form

$$f(J) = X_0 + X_1J + X_2J^2 + X_3J^3 + X_4J^4 + X_5J^5 + X_6J^6$$

was used and the coefficients are shown in Table VI.

TABLE VI

Expansion Coefficients for the P and R Branch Transitions

	P_{R_1}	R_{R_0}	R_{P_0}	R_{P_1} (u)	R_{P_1} (L)
X_0	0.66675330×10^{5}	$-0.66673097 \times 10^{5}$	0.61877906×10^{6}	0.48589794×10^{6}	0.48590642×10^{6}
X_1	0.51594239×10^{5}	0.51590030×10^{5}	$-0.51556174 \times 10^{5}$	$-0.51086247 \times 10^{5}$	$-0.51564556 \times 10^{5}$
X_2	$-0.25194343 \times 10^{3}$	0.25470597×10^{3}	0.24818775×10^{3}	0.21728078×10^{3}	$-0.25247593 \times 10^{3}$
X_3	$-0.68555273 \times 10^{0}$	$-0.12920792 \times 10^{1}$	0.10711691×10^{1}	0.42018117×10^{0}	$-0.10944739 \times 10^{0}$
X_4	$-0.63455543 \times 10^{-1}$	0.14714092×10^{0}	$0.70003528 \times 10^{-1}$	$0.82902655 \times 10^{-2}$	0.14977991×10^{0}
X_5	0	$-0.49850270 \times 10^{-2}$	$0.19754087 \times 10^{-2}$	$-0.15281750 \times 10^{-3}$	$-0.54692304 \times 10^{-3}$
X_6	0	$0.11485412 \times 10^{-3}$	$-0.48199598 \times 10^{-4}$	0	0

Over the range of the experimental data, these expressions are accurate to $\lesssim 1$ MHz and are substantially more straightforward to use than the theoretical formalism presented in the main body of this paper.

RECEIVED: December 3, 1979

REFERENCES

1. O. BAIN AND P. A. GIGUERE, *Canad. J. Chem.* **33,** 527–545 (1955).
2. D. CHIN AND P. A. GIGUERE, *J. Chem. Phys.* **34,** 690–691 (1961).
3. R. L. REDINGTON, W. B. OLSON, AND P. C. CROSS, *J. Chem. Phys.* **36,** 1311–1326 (1962).
4. R. H. HUNT, R. A. LEACOCK, C. W. PETERS, AND K. T. HECHT, *J. Chem. Phys.* **42,** 1931–1946 (1965).
5. J. T. MASSEY AND D. R. BIANCO, *J. Chem. Phys.* **22,** 442–448 (1954).
6. J. T. MASSEY AND D. W. HART, *J. Chem. Phys.* **23,** 942–946 (1955).
7. W. C. OELFKE AND W. GORDY, *J. Chem. Phys.* **51,** 5336–5343 (1969).
8. W. C. OELFKE, "Millimeter Wave Spectrum of Hydrogen Peroxide," Ph.D. thesis, Duke University, 1969.
9. P. HELMINGER, F. C. DE LUCIA, AND W. GORDY, *Phys. Rev. Lett.* **25,** 1397–1398 (1970).
10. G. WINNEWISSER, M. WINNEWISSER, AND W. GORDY, *J. Chem. Phys.* **49,** 3465–3478 (1968).
11. G. WINNEWISSER, *J. Chem. Phys.* **56,** 2944–2954 (1972).
12. G. WINNEWISSER AND P. HELMINGER, *J. Chem. Phys.* **56,** 2954–2966 (1972).
13. G. WINNEWISSER AND P. HELMINGER, *J. Chem. Phys.* **56,** 2967–2979 (1972).
14. F. C. DE LUCIA AND P. HELMINGER, *J. Mol. Spectrosc.* **54,** 200–214 (1975).
15. J. K. G. WATSON, *J. Chem. Phys.* **45,** 1360–1361 (1966).